

Beam focusing in reflection from flat chirped mirrors

Y. C. Cheng,¹ M. Peckus,² S. Kicas,² J. Trull,¹ C. Cojocaru,¹ R. Vilaseca,¹ R. Drazdys,² and K. Staliunas^{1,3}

¹*Departament de Física i Enginyeria Nuclear, Universitat Politècnica de Catalunya, Colom 11, 08222 Terrassa, Barcelona, Spain*

²*Center for Physical Sciences and Technology, Savanoriu Ave. 231, LT-02300, Vilnius, Lithuania*

³*Institució Catalana de Recerca i Estudis Avançats (ICREA), Pg. Lluís Companys, 23, 08010 Barcelona, Spain*

(Received 21 December 2012; published 15 April 2013)

We propose and show by proof-of-principle calculations and experiments that beam focusing and imaging can be obtained in reflection from a flat interface of a micromodulated dielectric structure. We show, in particular, that a one-dimensionally modulated and chirped structure can focus a beam, performing an imaging of a light pattern, i.e., can act as a transversely invariant flat focusing mirror.

DOI: [10.1103/PhysRevA.87.045802](https://doi.org/10.1103/PhysRevA.87.045802)

PACS number(s): 42.25.Fx, 42.55.Tv, 42.79.—e

Spatially micromodulated materials such as photonic crystals (PhCs) are known to be able to substantially modify the flow of light inside and behind the material in both frequency and spatial domain [1,2]. Particularly, spatial dispersion (diffraction) of beams can be suppressed or even made negative, leading to *flat lens* focusing and imaging in transmission through PhCs [3,4]. A flat PhC lens, consisting of a very thin slice of PhCs, can focus a beam or form light-pattern image, even with a subwavelength resolution [5,6]. Furthermore, optical metamaterials designed for negative refraction [7,8] have also been proposed for flat lensing with usual- and subwavelength resolution. The translational invariance of flat lenses in transverse direction (on a spatial scale larger than the transverse modulation period) makes them principally different from the standard curved-surface or diffractive lenses, and even from the recently proposed flat lenses based on nanoantenna arrays [9], as the latter ones always possess an optical axis and thus require a precise steering and lateral positioning of the incident beam.

In this Brief Report we show the effects of beam focusing and light-pattern imaging, with transverse invariance, by means of a flat photonic structure working in reflection instead of transmission. The principle of flat lensing in transmission relies on negative spatial dispersion of wave propagating in the material, meaning that the plane-wave components at larger angles get larger phase delays propagating through the material. For normal dispersion, in vacuum, the angular dependence of phase delay is opposite. The concept of a flat focusing mirror in reflection also should rely on the negative spatial dispersion: The reflection should change the phases of the plane-wave components so that waves at a larger incidence angle would get larger phase delay in reflections. This effect is impossible in reflections from a usual metallic or dielectric mirror, where the waves reflect directly from the interface. Such usual reflection results in angle-independent phase delays, and eventually in zero spatial dispersion. The dispersion, however, could be in principle manipulated if the reflecting wave would penetrate substantially deep into the structure, and, importantly, if the penetration depth would depend on the incidence angle.

The wave reflecting from chirped photonic structures can indeed reflect from the different depth, as shown in Fig. 1. This brings us to an idea, that chirped PhCs could provide negative spatial dispersion, and consequently, can lead to the concept

of a flat focusing mirror. We consider here the simplest case of a one-dimensional (1D) quasiperiodic dielectric structure made of alternating layers of different refractive index, with the spatial period varying with the penetration depth. It is known that at normal incidence the penetration depth of plane waves is *frequency* dependent since the local frequency of the photonic band gap depends on the longitudinal position within chirped structures [10]. In the case of a positive sign of the chirp (lattice period decreases with penetration distance) waves at higher frequencies penetrate deeper into the structure and thus experience larger phase and group-velocity delays, as shown in Fig. 1(a). This effect is readily used to correct material dispersion in femtosecond lasers (double chirped mirror [11]).

If we consider different *incidence angle* instead of different frequency [Fig. 1(b)], plane-wave components will also reflect at different depths. This happens because plane waves at larger incidence angles have a shorter longitudinal component of the wave vector, so their propagation and reflection is equivalent to that of the waves of lower frequency at normal incidence. Since the waves will follow paths with different optical lengths, this will result in angular-dependent phase delays. These delays can lead to negative spatial dispersion and to beam focusing or imaging, as qualitatively illustrated in Fig. 1(c). Here a beam focused in front of the structure undergoes positive spatial dispersion before reflection, negative dispersion inside the structure during reflection, and again positive spatial dispersion propagating in free space after reflection. The free-space positive dispersion balances the negative dispersion in the structure and leads to focusing of the beam at a certain distance from the mirror. Note that in the configuration of a longitudinally chirped 1D structure the focusing effect is expected to occur only within the plane of incidence, so that the beam cross section at the output is expected to become elliptic.

To substantiate the idea, we consider a 1D modulated structure with positive linear chirp coefficient ($\alpha > 0$) characterized by a Bragg spatial frequency depending on the longitudinal coordinate z [$k_B(z) = k_0 + \alpha z$, $k_0 = \omega_0/c$ being the Bragg spatial frequency at the entrance]. Rough estimation of the character of reflection can be obtained assuming that each plane-wave component of the incident beam is reflected approximately where the Bragg resonance occurs. The pulses of a plane wave with the wave vector centered around $\vec{k} = (k_x, k_z)$ (k_x and k_z being its transverse

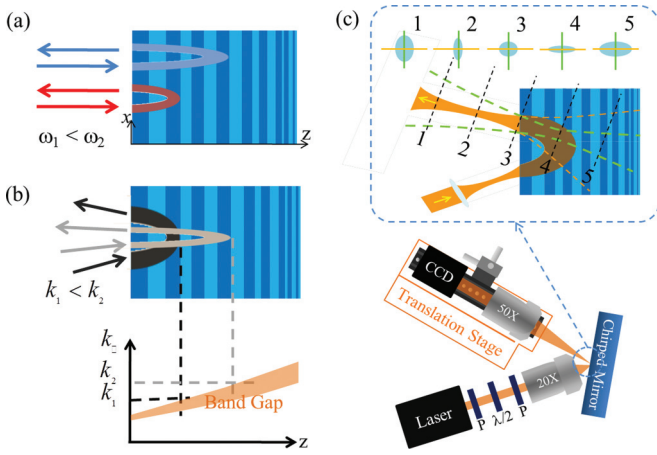


FIG. 1. (Color online) Principle of a 1D chirped mirror: (a) Normal incidence: plane waves of higher frequency (ω_1 , blue color) penetrate deeper into the structure because of the space dependence of the frequency of band gap. (b) Oblique incidence: plane waves at smaller incidence angles (larger longitudinal wave vector, k_1 , gray color) penetrate deeper into the structure. (c) Expected scenario for the focalization of light beams. The insets represent the expected intensity cross section at different positions 1, 2, 3, ... along the reflected beam. The dashed line indicates approximately the beam divergence in the case of usual reflection of the same beam. (d) Experimental setup used to observe the cross sections of the reflected beam at different positions (cw diode laser at $\lambda = 532$ nm, polarizers P, $\lambda/2$ plate, 20 \times and 50 \times objective lenses, CCD camera, and translation stage).

and longitudinal components) reflects approximately at a depth $l = (k_z - k_0) / \alpha$ of the structure, so that the accumulated group delay along the total forward-backward reflection path is $2l = 2(k_z - k_0) / \alpha$. The group delay is, by definition, the derivative of the field phase with respect to k_z ; i.e., $2l \equiv d\varphi / dk_z$, and can be calculated by simple integration of the accumulated phase shift of the reflected plane wave: $\varphi(k_z) \approx k_z(k_z - 2k_0) / \alpha$. The derivative of the phase versus k_x gives the lateral shift of the beam, $s = -d\varphi / dk_x$ (also called the Goos-Hänchen shift [12,13]), whereas the second derivative of the phase versus k_x determines the diffractive broadening of the beam. The latter can be characterized by means of a “diffractive propagation

distance” $L_{\text{diff}} = -kd^2\varphi / dk_x^2$ which gives an equivalent beam propagation distance in vacuum. In other words, the L_{diff} with negative sign: $-L_{\text{diff}} = kd^2\varphi / dk_x^2$ has a meaning of a focal length of flat focusing mirror. Taking into account the evident relation between the longitudinal and transverse wave-number components $k^2 = k_x^2 + k_z^2$, we obtain

$$s = -\frac{d\varphi}{dk_x} = \frac{2}{\alpha} \left(k - k_0 - \frac{1}{2} \frac{k_x^2}{k} \right) \frac{k_x}{k}, \quad (1a)$$

$$L_{\text{diff}} = -k \frac{d^2\varphi}{dk_x^2} = \frac{2}{\alpha} \left(k - k_0 - \frac{3}{2} \frac{k_x^2}{k} \right). \quad (1b)$$

These expressions show that for a positive chirp and for $k > k_0$, a negative spatial dispersion length, which entails focusing of the beam, can be expected at sufficiently large incidence angles.

We have checked this very rough analytical estimation by numerical calculations considering a concrete 1D chirped structure consisting of 20 periods of two alternating dielectric layers with low ($n_1 = 1.5$) and high ($n_2 = 2.17$) refractive indices. The layer thickness sweeps from $d_1 = 118$ nm, $d_2 = 88$ nm at the entrance of the mirror (Bragg wavelength is 736 nm) to $d_1 = 89$ nm, $d_2 = 66$ nm at the rear face (Bragg wavelength is 553 nm). A standard transfer matrix method has been used to calculate the amplitude and phase of the reflection coefficient for this structure.

Figure 2 shows the angular dependence of the lateral beam shift s and the diffractive propagation distance L_{diff} (continuous lines), respectively, for both polarizations of the incident wave. Both plots show the expected tendencies according to our analytical estimations (1), also represented by dashed lines. The expected tendencies, however, are strongly overlaid by a fringe structure. The origin of these fringes lies in the coupling between the forward and backward waves due to the periodicity of the structure [14]. This fringing effect can be controlled by modifying the chirp function. However, importantly, at particular angular ranges, the fringes strongly increase the searched effect of negative diffraction, as seen in Fig. 2(c). The L_{diff} thus becomes strongly negative, and the searched effect becomes even substantially larger than analytically estimated (1). We note that the fringes for two different polarizations appear shifted in angular domain, as

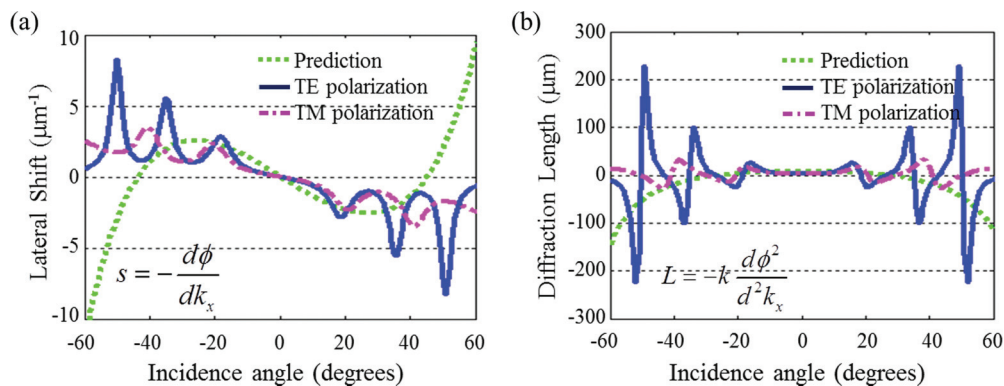


FIG. 2. (Color online) Angular dependence of the reflection properties of the chirped structure: (a) lateral shift of the light beam, $s = -d\varphi / dk_x$; (b) spatial dispersion (diffractive propagation) distance $L_{\text{diff}} = -kd^2\varphi / dk_x^2$. Results for TE and TM polarization are given by blue and red-dashed lines, correspondingly; analytical estimations from (1) are depicted by green-dotted lines.

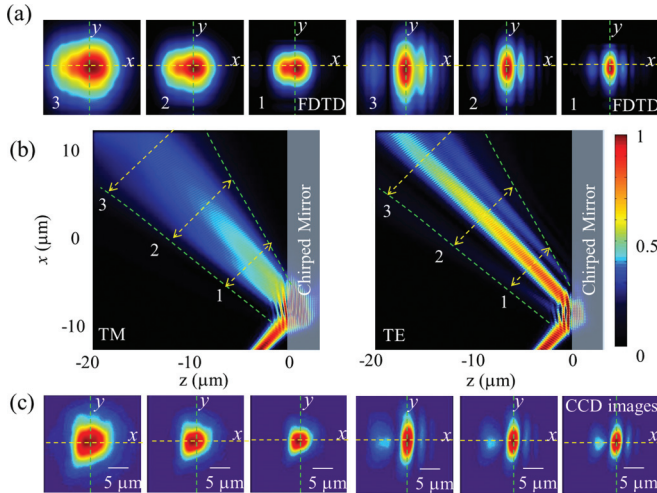


FIG. 3. (Color online) Beam reflection from 1D chirped structure considered in Fig. 2, for TM (left pictures) and TE (right pictures) polarization, at a particular incidence angle of 54° : (a) beam profile within the plane of incidence; [(b),(c)] beam cross sections at the corresponding transverse planes 1, 2, and 3 indicated in (a). (a) and (b) show the FDTD calculations, and (c) shows the experimental CCD images. As a reference, the broadening of the same beam reflecting from a metallic mirror is also plotted (green dashed line).

the reflection coefficients are different for both polarizations for nonzero incidence angles.

Global pictures of beam reflection were obtained by numerical calculation using the finite difference time domain (FDTD) method in two-dimensional (2D) space. The results for the structure described previously are shown in Fig. 3. The beam was focused at a distance of $5 \mu\text{m}$ in front of the chirped mirror reaching a beam waist diameter $w_0 = 2 \mu\text{m}$, which corresponds to a Rayleigh length of $6 \mu\text{m}$, for $\lambda = 532 \text{ nm}$ radiation. The particular incidence angle of 54° corresponds to the deepest fringe of negative dispersion shown in Fig. 2(c). A clear focalization is obtained for the reflected TE polarized beam. The wave fronts of that beam are concave (converging) right after the reflection, so that the intensity along the axis of the reflected beam gets a maximum at a certain distance. In Fig. 3(b) we show three perpendicular cross sections of the reflected beam, at different positions. The beam profiles for TE polarization clearly show an elliptic shape with the shorter axis within the incidence plane (since the focusing effect appears only in that direction). In contrast, for TM polarization this focusing effect does not appear at this particular incidence angle, and the beam profiles are similar to reflecting from a usual metallic mirror.

In order to prove experimentally the predicted effect, we have built a 1D chirped mirror, and focused a beam of cw laser in front of the structure, as schematically shown in Fig. 1(d). The samples were vacuum vaporized on fused silica substrates by ion beam sputtering technique. The layers of higher and lower refractive index materials were vaporized in alternating order: The high refractive index material was ZrO_2 , $n = 2.17$, and the low refractive index material was SiO_2 , $n = 1.5$. The thicknesses of growing layers were monitored by an integrated broadband transmission optical monitoring system.

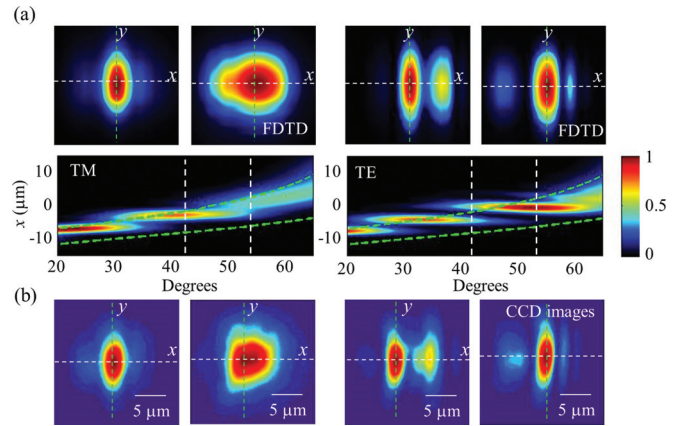


FIG. 4. (Color online) FDTD simulations of beam reflection from the 1D chirped structure considered in Fig. 2, for TM (at the left) and TE (at the right) polarization: (a) the vertical cuts at a distance $z = -5 \mu\text{m}$ with different incident angles; (b) beam cross sections for two particular incidence angles of 42° and 54° are plotted. These two angles are indicated in (a) by vertical dashed lines. The green dashed lines in (a) represent the position and width (at $1/e^2$ intensity level) of the beam reflected on a metallic mirror; (c) experimental CCD images obtained for equivalent conditions.

All parameters of the samples correspond to those used in FDTD calculations.

The reflected beam transverse profile was imaged into a CCD camera. Figure 3(c) shows the recorded images, at the same distances from the mirror surface as in the numerical calculations. The predicted behavior [Fig. 3(b)] is reproduced: The reflected beam cross sections are ellipses with the in-plane-of-incidence axis shorter than the perpendicular one. The vertical cross section of the 2D beam images has approximately the same size as in reflection from a normal metallic mirror. For TM polarization no negative diffraction effect is observed at this particular angle, exactly as in numerical results.

The focusing depends on the incidence angle, with areas of negative L_{diff} values (focusing) alternating with areas of positive L_{diff} (defocusing). To check this scenario we fixed an observation plane parallel to the mirror's face ($z = -5 \mu\text{m}$), and recorded the transverse beam profiles for different incidence angles. Figure 4 summarizes numerical [Figs. 4(a) and 4(b)] and experimental [Fig. 4(c)] results. Figure 4(a) shows that the focusing is strongly dependent on the incidence angle, indicating particular ranges where the effect is more pronounced. We focus on two particular angles: 42° and 54° [vertical dashed lines in Fig. 4(a)]. Figure 4(b) shows strong focusing for TE polarization at 54° (ellipse compressed in the x direction) and practically no effect for TM polarization. In contrast, at 42° the scenario changes resulting in strong focusing or collimation for TM polarization (with a single dominant elliptic profile) and focusing with fringes (two comparable elliptic profiles close to each other) for TE polarization. The corresponding experimental images shown in Fig. 4(c) confirm these scenarios. The dependence of the lateral shift of the beam on the incidence angle is also clearly visible from the map.

In conclusion, we predict and experimentally demonstrate the modification of the diffractive spreading of light beams upon reflection from flat interfaces of photonic microstructures. The possibility to obtain negative diffraction leads to the concept of flat focusing- or real-imaging flat mirror. The system is invariant with respect to lateral translations of the incident beam, and can image an incident light pattern. The flat focusing mirror effect has been demonstrated here only for a 1D modulated structure with a linear chirp, providing a proof-of-principle study. The demonstration shows some apparent limitations: focalization appears only at nonzero incidence angles, it is not monotonic with respect to the angle (fringing effects), and it occurs only in one lateral direction. Nevertheless, significant improvements could be obtained, for instance, by optimizing the chirp function in order to

reduce or increase (depending on the applications) the fringing; considering three-dimensional (3D) mirror geometries, as e.g., a 90° three-mirror corner; moving to 2D and 3D PhCs to modify the angular ranges of negative diffraction, and to extend the application to normal incidence. This effect opens new possibilities to beam manipulation in microphotonic circuits as, for example, to build microcavities or microlasers with focusing flat end mirrors.

We acknowledge financial support by Spanish Ministerio de Educación y Ciencia and European FEDER (project FIS2011-29734-C02-01), Generalitat de Catalunya (2009 SGR 1168), and by European Union Structural Funds project “Postdoctoral Fellowship Implementation in Lithuania”.

-
- [1] S. John, *Phys. Rev. Lett.* **58**, 2486 (1987).
 [2] E. Yablonovitch, *Phys. Rev. Lett.* **58**, 2059 (1987).
 [3] P. V. Parimi, W. T. Lu, P. Vodo, and S. Sridhar, *Nature (London)* **426**, 404 (2003).
 [4] C. Luo, S. G. Johnson, J. D. Joannopoulos, and J. B. Pendry, *Phys. Rev. B* **65**, 201104 (2002).
 [5] E. Cubukcu, K. Aydin, E. Ozbay, S. Foteinopoulou, and C. M. Soukoulis, *Nature (London)* **423**, 604 (2003).
 [6] Z. Lu, J. A. Murakowski, C. A. Schuetz, S. Shi, G. J. Schneider, and D. W. Prather, *Phys. Rev. Lett.* **95**, 153901 (2005).
 [7] V. G. Veselago, *Sov. Phys. Usp.* **10**, 509 (1968).
 [8] J. B. Pendry, *Phys. Rev. Lett.* **85**, 3966 (2000).
 [9] F. Aieta, P. Genevet, M. A. Kats, N. Yu, R. Blanchard, Z. Gaburro, and F. Capasso, *Nano Lett.* **12**, 4932 (2012).
 [10] R. Szipöcs, K. Ferencz, C. Spielmann, and F. Krausz, *Opt. Lett.* **19**, 201 (1994).
 [11] M. Matuschek, F. X. Kärtner, and U. Keller, *IEEE J. Sel. Top. Quantum Electron.* **4**, 197 (1998).
 [12] F. Goos and H. Hänchen, *Ann. Phys.* **436**, 333 (1947).
 [13] R. H. Renard, *J. Opt. Soc. Am.* **54**, 1190 (1964).
 [14] A common opinion is that the fringes appear as the result of the interference between the waves reflected from the front face, and from some position in the bulk of the crystal (the position where the wave “enters” into “band gap” and reflects). This reason for fringing, however, can be easily eliminated by introducing antireflection coatings. Another reason for fringing is the interaction between forward and backward propagating waves in a bulk of the structure. The bulk fringing is not so easy to eliminate, and requires a separate study.